Amelogenin Nanoparticles in Suspension: Deviations from Spherical Shape and pH-Dependent Aggregation

Barbara Aichmayer,*,† Felicitas B. Wiedemann-Bidlack,‡ Christoph Gilow,† James P. Simmer,§ Yasuo Yamakoshi,§ Franziska Emmerling,⊥ Henry C. Margolis,*,‡ and Peter Fratzl†

Department of Biomaterials, Max Planck Institute of Colloids and Interfaces, D-14424 Potsdam, Germany, Department of Biomineralization, The Forsyth Institute, Boston, Massachusetts 02115, Dental Research Laboratory, University of Michigan, Ann Arbor, Michigan 48109, and BAM Federal Institute for Materials Research and Testing, D-12489 Berlin, Germany

Received August 27, 2009; Revised Manuscript Received November 25, 2009

It is well-known that amelogenin self-assembles to form nanoparticles, usually referred to as amelogenin nanospheres, despite the fact that not much is known about their actual shape in solution. In the current paper, we combine SAXS and DLS to study the three-dimensional shape of the recombinant amelogenins rP172 and rM179. Our results show for the first time that amelogenins build oblate nanoparticles in suspension using experimental approaches that do not require the proteins to be in contact with a support material surface. The SAXS studies give evidence for the existence of isolated amelogenin nano-oblates with aspect ratios in the range of 0.45−0.5 at pH values higher than pH 7.2 and show an aggregation of these nano-oblates at lower pH values. The role of the observed oblate shape in the formation of chain-like structures at physiological conditions is discussed as a key factor in the biomineralization of dental enamel.

Introduction

Dental enamel, the most highly mineralized structure in the vertebrate body, consists of well-ordered arrays of enamel prisms that are each constructed of parallel bundles of high aspect-ratio carbonated hydroxyapatite crystals.[1] Unraveling the mechanisms behind the formation of this sophisticated, hierarchical structure is of great interest with respect to understanding the basis of malformed tooth enamel and the development of new bioinspired materials for enamel tissue regeneration and repair.

Whereas the migration of ameloblast cells is of crucial importance for controlling the structural arrangement of enamel on the micrometer scale and above,[2] the elongated growth and parallel alignment of the mineral crystals on the length scale of nanometers is mainly determined by the interaction with amelogenin proteins and their self-assembly.[1,3] Amelogenins comprise about 90% of all proteins secreted by ameloblast cells.[4] During the secretory stage of amelogenesis, long thin ribbons of enamel mineral crystals are formed almost immediately as the ameloblast lays down enamel matrix proteins, suggesting that enamel mineralization does not take place within a preformed matrix.[1] Interestingly, the pH within secretory enamel has been found to be close to neutrality and within a narrow range, with average values of pH 7.26 in the pig[5] and pH 7.23 in the rat.[6] As the enamel tissue matures, enamel matrix proteins are successively degraded[7–9] and removed, allowing the initial mineral crystals to grow in thickness and in width to produce an enamel layer that is >95% mineral by weight.[3]

Transmission electron microscopy (TEM) investigations of developing rat incisor enamel[10] using a freeze-fracture technique revealed that the forming region (youngest enamel) consisted of globular structures with a diameter of 30−50 nm that were either randomly or linearly arranged. At a somewhat later stage of development, these globules appeared to be more linearly arranged. In regions approaching enamel maturation, mineral crystallites that were 50−60 nm wide and 5−6 nm thick were found as closely packed bundles that were 4 μm in diameter.[10] These bundles were assumed to correspond to the enamel prisms. Based on these observations, the authors concluded that the organized globules played a role in the ordered growth of enamel crystals. In vitro studies later demonstrated that recombinant murine amelogenins form spherical structures[11,12] with dimensions similar to those of the globules observed in developing rat enamel.[10] Based on a comparison of observations from TEM studies on mouse, bovine, and hamster enamel, amelogenin nanospheres were postulated to be the main functional component controlling the crystal growth and spacing in the forming enamel.[13] The self-assembly of recombinant and native amelogenins into nanospheres has been thoroughly investigated by means of dynamic light scattering (DLS)[12,14,15] in combination with atomic force microscopy (AFM)[15,16] and also using TEM.[11,17] Our own previous in vitro studies combined DLS and small-angle X-ray scattering (SAXS)[18] to investigate the recombinant full length murine amelogenin rM179 and its cleavage product rM166, which lacks the hydrophilic C-terminus found in the full-length molecule. The results confirmed the existence of nanosized amelogenin agglomerates in suspensions and supported a core−shell model for full-length amelogenin, where the hydrophobic portion of the protein makes up the dense inner part and the hydrophilic portions corresponding to the charged C terminus build a loose shell around this core. Furthermore, we observed a temperature-induced onset of aggregation of the amelogenin nanoparticles in suspension, which was strongly influenced by the presence of the charged C-terminus.[18] When the same general approach is used,

* To whom correspondence should be addressed. E-mail: aichmayer@mpikg.mpg.de (B.A.); hmargolis@forsyth.org (H.C.M.).
† MPI of Colloids and Interfaces.
‡ The Forsyth Institute.
§ University of Michigan.
⊥ BAM.

10.1021/bm900983b
Published on Web 12/28/2009

combined DLS and TEM observations on the pH and temperature-dependent self-assembly of murine and porcine amelogenins highlighted the importance of the pH value for triggering the aggregation process. The full length proteins rP172 and rM179 were found to form higher-order assemblies at pH 7.2.[19] Such higher-order assembly observed by TEM was described as a linear aggregation of nanospheres to form chains.[19–21]

Except for the DLS studies, the results on the assembly of amelogenin into nanospheres and their aggregation to build chains, as described above, were obtained using approaches (i.e., TEM and AFM) where proteins were immobilized on solid substrates and dried prior to analyses. For characterization by means of TEM and AFM, the suspensions were put on mica surfaces, TEM grids, or similar support materials. However, the structure of the protein nanoparticles is very likely affected by such underlying support materials and drying. Hence, it is very difficult to obtain detailed information on the three-dimensional (3D) shape of amelogenin nanoparticles by such direct imaging techniques without inducing possible artifacts. An AFM study[16] has reported deviations from the frequently described spherical shape, toward a more flat appearance, when fixed samples of rM179 were examined on mica surfaces, although this point or its potential importance was not discussed further. Other studies have described amelogenin aggregates formed from mixtures of porcine amelogenins[22] and from solutions of recombinant mouse amelogenins[13,14] as being "quasi-spherical", based on TEM and AFM analyses. However, the meaning or relevance of this nanoparticle description was not discussed. Nevertheless, it remains that the true nature of amelogenin nanospheres in suspension has not been fully characterized. DLS studies, which are based on the diffusion behavior of the particles in suspension, have provided information on the size of amelogenin nanoparticles and have shown that they are monodispersed[12,18] under specified conditions. However, such analyses do not provide any details on their true shape. When SAXS is used, the 3D structure of amelogenin nanoparticles in suspension can be characterized, as our previous SAXS studies on recombinant murine amelogenins[18] have shown. This initial study provided evidence that clearly suggested that the full-length recombinant murine amelogenin formed nanoparticles that deviated from a spherical shape. The current paper focuses on furthering such studies by describing the shape of both porcine and murine amelogenin nanoparticles and their pH-dependent aggregation by means of SAXS.

Materials and Methods

Protein Preparation. Recombinant murine and porcine amelogenins rM179 and rP172 were produced in bacteria and purified as previously described.[23] In contrast to their native counterparts, the recombinant amelogenins lack the N-terminal methionine as well as a single phosphate group at serine-16.

Protein Solution Preparation. Stock solutions with a concentration of 5 mg/mL were made by dissolving lyophilized proteins in ice-cold distilled deionized water. The stock solutions were then stored for at least 24 h at 4 °C prior to use. Experimental solutions with concentrations of 2 mg/mL protein and 80 mM Tris-HCl at selected pH values were then prepared on ice by diluting protein stock solutions with buffers that had been preadjusted to desired pH values at either 25 or 37 °C (different values in the range of pH 7−7.8 at 25 °C and pH 7.2 at 37 °C). All buffer solutions and water were filtered prior to use. The temperature dependence of the Tris-HCl buffer was used to change the pH of the protein suspensions by means of varying the temperature between 4 and 37 °C. The pH values given in the tables and graphs were either measured or calculated using the known temperature dependence of $\Delta pH = -0.03/°C$. It has previously been shown that measured and calculated pH values are in a good agreement.[19]

SAXS—Instrumentation. For the SAXS experiments a Nanostar laboratory instrument (Bruker AXS, Karlsruhe, Germany) was used. It consists of a sealed X-ray tube which operates at 1.5 kW (40 kV, 35 mA, Cu Kα, $\lambda = 1.54$ Å), a pair of cross coupled Göbel-mirrors for monochromatization and parallel focusing, three pinholes (∅ 750 μm, 400 μm defining the beam size and 1000 μm to suppress scattering from the second pinhole) and a position sensitive two-dimensional area detector (HI-STAR, Bruker AXS). The pinholes as well as the sample and the detector were kept under vacuum during the experiment. Transmissions were measured indirectly by using a glassy carbon standard, which gives a very strong scattering signal that is proportional to the transmitted intensity. The protein solution was contained in a vacuum-sealed quartz glass capillary with a diameter of 1.5 mm (Anton Paar, Graz, Austria), which was mounted on a Peltier-element (TCU 50, Anton Paar) to vary the temperature of the sample. The protein was measured at three distinct temperatures: 4, 25, and 37 °C during heating and again at 4 °C after cooling. After each temperature step, measurements were taken with increasing acquisition times (starting with 1000 s exposure time). For those experiments where the pH dropped to 7.2 or below when the temperature was increased, we observed time-dependent changes when comparing the data sets measured during the first 4 h. When the scattering signal did not change anymore, measurements with longer acquisition times (∼3−6 h) were done to improve the statistics. Only the data collected after the initial equilibration time of up to 4 h was used for further evaluation.

In addition to the laboratory experiments, concentration dependent measurements were carried out at the μ-Spot beamline[24] at BESSY II (Berlin, Germany) using a two-dimensional MarMosaic CCD detector (Mar 225, Mar, Evanston, U.S.A.). The beam was monochromatized using a Si 111 double-crystal monochromator. Harmonics were suppressed and the beam was focused by a curved mirror. The focusing scheme of the beamline is designed to provide a divergence <1 mrad (horizontally and vertically) and a beam diameter of roughly 20 μm at a photon flux of 1×10^9 s^{-1} at a ring current of 100 mA. The experiments were carried out employing a wavelength of 1.003 Å. The sample was a free floating droplet of protein solution in an ultrasonic trap (Tec5, Oberursel, Germany). The ultrasonic trap (operating at 58 kHz and a sound level of 156 dB) creates a standing acoustic wave between a transmitter and a reflector with equidistant nodal points in which droplets can be held. The ultrasonic field causes air-convection which induces stirring of the droplet, thus ensuring a homogeneous concentration distribution within the sample. The scattering patterns were collected while the solvent slowly evaporated. We measured a 5 μL droplet of a 2 mg/mL suspension of rP172 80 mM Tris-HCl adjusted to pH 7.8 at 25 °C. SAXS measurements were taken in 150 s intervals until the solvent was completely evaporated (after 42 min). The evaporation caused an increase in the protein concentration that was calculated assuming a linear decrease of the droplet radius with time. This is well in agreement with previous experimental observations.[25] The linear decrease of the radius corresponds to a constant evaporation rate per surface area and time. Temperature control was not available for this setup, so the experiments were carried out at room temperature (∼20 °C), where the measured pH of the protein suspension was pH 7.9.

SAXS—Evaluation. Azimuthal integration of the isotropic two-dimensional scattering signals using the program FIT2D (A. Hammersley, ESRF, Grenoble, France) gave the scattered intensity as a function of the modulus of the scattering vector Q ($Q = 4\pi \sin(\theta)/\lambda$, where λ is the wavelength and 2θ is the scattering angle). The scattering intensities were then corrected for background scattering of the pinhole, the capillary, and the solvent, taking into account the transmission of the sample. Distilled water was used as a secondary standard to convert the measured scattering intensities into scattering cross sections per unit volume.[26]

For systems in which interparticle interferences can be neglected, the SAXS signal can be described by the Guinier approximation $I(Q) = I_0\exp(-Q^2R_g^2/3)$ for small Q values ($QR_g < 1-2$).[27] $I(Q)$ is the scattering cross section per unit volume, I_0 is the limit of $I(Q)$ for $Q \rightarrow 0$ and R_g is the radius of gyration defined as $R_g^2 = (\int_V r^2\rho(r)dV)/(\int_V \rho(r)dV)$. Guinier plots ($\ln[I(Q)]$ vs Q^2) and linear regressions were used to evaluate the size parameter R_g. The errors were derived from the calculated errors of the linear regressions in the Guinier plots which were done for the Q-range between 0.13 nm^{-1} and 0.26 nm^{-1}.

Modeling of the SAXS profiles was done using the following fitting function for monodisperse ellipsoids of revolution with the semiaxis $R_1 = R_2 = R$ and $R_3 = R\varepsilon$:[28] $I(Q,R,\varepsilon,I_0) = N(\Delta\rho)^2V^2 \int_0^{\pi/2} F_s^2[Q,r(R,\varepsilon,\alpha)] \sin(\alpha)d\alpha$, where $r(r,\varepsilon,\alpha) = R(\sin^2\alpha + \varepsilon^2\cos^2\alpha)^{1/2}$ and $F_s(Q,r) = 3[\sin(Qr) - Qr\cos(Qr)]/(Qr)^3$. N is the number of independently scattering particles, $\Delta\rho$ the difference in the scattering length densities of the particles and the solvent, and V corresponds to the volume of each of the particles. We used oblate ellipsoids ($\varepsilon < 1$) to model the scattering profiles of both rM179 and rP172. The data were fitted numerically with Mathematica 5.2 (Wolfram Research, Champaign, IL, USA) by a least-squares method using the inverse error of the scattering cross sections as weights. The parameter χ^2_{red}[28] was used as an indicator for the quality of the fit. $\chi^2_{red} = 1$ corresponds to an ideal fit, where the average deviation between the fitted function and the data points is equal to the statistical error of the measured data. We also compared our data with monodisperse spherical particles ($\varepsilon = 1$) and spheres with a Gamma size distribution: $f(R,\gamma,\alpha) = \gamma^\alpha R^{\alpha-1}\exp(-\gamma R)/\Gamma(\alpha)$, $I(Q,R,\gamma,\alpha) = \int_0^\infty I[Q,R]f(R,\gamma,\alpha)dR$. Only for reasons of comparison and to see how strongly a moderate polydispersity would affect the results obtained with the monodisperse oblate model, we also combined the two approaches (fitting the parameters R and ε, R having a Gamma size distribution with a fixed polydispersity of 15%).

The molar mass M_w of the particles was calculated from the forward intensity $I_0 = N(\Delta\rho)^2V^2 = M_wc(\rho_p - \rho_s)^2/(N_A\delta_p^2)$, which depends on the protein concentration c, the mass density of the protein δ_p, and the contrast between the solvent and the protein $(\rho_p - \rho_s)^2$, N_A is Avogadro's number, and all other parameters have the same meaning as described above. The following estimated average values for the protein were used: $\delta_p = 1.44$ g/cm^3, calculated using an approximation that relates the molecular mass of the proteins (about 20 kDa for rM179 and rP172, see below) to their average mass density[29] and $\rho_p = 11.8 \times 10^{14}$ m^{-2}.[26] The buffer solution is primarily water with a scattering length density of $\rho_s = 9.43 \times 10^{14}$ m^{-2}. Dividing the molar mass of the particle M_w by the molar mass of the protein monomer M_P, which corresponds to 19574 g/mol and 20161 g/mol for rP172 and for rM179, respectively,[30] gave the number n of amelogenin monomers per particle.

DLS. DLS data were collected using a DynaPro MSXTC/12 instrument with a gallium-arsenide diode laser (DynaPro-99-E-50) of 825.2 nm emission and programmable power. The instrument has a temperature-controlled sample holder (precision of 0.1 °C) for a quartz cuvette of 12 μL. Scattering data were collected at an angle of $\theta = 90°$ and processed using the software program DYNAMICS V6, version 6.3.40. A regularization algorithm was used to resolve for up to five multimodal populations and their polydispersity, normalized to the mean size of the peak and the hydrodynamic radius (R_H). All R_H data reported here were modeled as isotropic spheres and result from mass-weighted calculations. Mass-weighted calculations were used, because DLS is a method that is very sensitive to large particle sizes. Polydispersity is defined as the relative standard deviation of R_H measurements and expressed as percent polydispersity (%PD). In agreement with a previously developed convention based on comparing the %PD as measured by DLS with gel electrophoresis analyses (SDS-PAGE)[31] and the ease of crystallization of proteins,[32] populations with a polydispersity <15% are considered monodisperse, whereas those with values >15% are considered polydisperse.

DLS data were collected for 2 mg/mL samples of rM179 and rP172 prepared in 80 mM Tris-HCl buffers adjusted to pH 7.2 at 37 °C. Data were collected as a function of pH between pH 8 and pH 7 by increasing the temperature from 7 to 43 °C. Each sample was allowed to equilibrate at a given temperature for 5 min. The ensuing measurements consisted of 20 acquisitions of 5 s each and were repeated three times at the same temperature in 5 min intervals. Consequently, each sample was kept at any given temperature for more than 20 min, allowing us to check for particle size changes during the period of data collection at each temperature. More than 95% of the measurements did not show any sizable second population with a mass fraction >1%. A total of 8 out of 188 measurements for rM179 and rP172, which did show a significant second population, were disregarded for further evaluation, because for each of them three other measurements within the 20 min showed only one (100% by mass) population. Due to its very rare and transient occurrence, the second population is not considered relevant for the comparison with SAXS data collected using much longer acquisition times of hours.

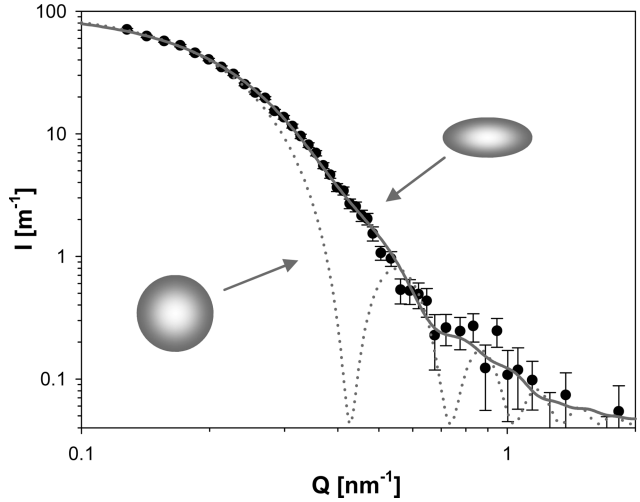

Figure 1. Small-angle X-ray scattering (intensity I vs modulus of the scattering vector Q) of rP172 (2 mg/mL) in 80 mM Tris-HCl at 4 °C and a measured pH value of 8.1. The experimental data, collected with a Nanostar laboratory instrument, correspond to the black dots with error bars and are not consistent with the scattering function for monodisperse spheres (dotted gray line, calculated for spheres of 10.5 nm in radius, 0%PD). The solid gray line shows a fit with the scattering function for monodisperse (0%PD) oblate ellipsoids, which describes the data very well. The fitted size parameters were 5.5 and 12.2 nm for the shorter (= rotational) and longer half axes, respectively.

Results

In the investigated range of pH values between pH 7 and pH 8.1, both recombinant proteins formed aggregates that gave rise to a pronounced small-angle scattering intensity in the observed Q range of 0.13−2 nm^{-1}. Figure 1 shows a typical example for a scattering profile of rP172, measured at pH 8.1 and a temperature of 4 °C.

A comparison of the experimental data with the scattering function of monodisperse spheres (see the dotted gray line, $R = 10.5$ nm, 0%PD) shows that such a simple model is not suitable for describing the observed small-angle scattering behavior. Monodisperse spherical particles would give rise to oscillations in the small-angle scattering intensity, as illustrated, which we did not observe. Taking into account a possible deviation from the spherical shape, scattering functions for ellipsoids were fit to the data. A fit with monodisperse oblate (flat) particles turned out to be in excellent agreement with the measured scattering data (see the full gray line in Figure 1, $\chi^2_{red} = 1.09$, 1 being an ideal fit). All scattering profiles of rP172 and rM179 that were measured at pH values larger than pH 7.2

Table 1. Length of the Larger Half Axes ($R_1 = R_2$), the Shorter Half Axis (R_3), Aspect Ratio (R_3/R_1), and Number of Protein Monomers (n) per Nano-Oblate (0%PD), Evaluated from SAXS Data Measured Using a Nanostar Laboratory Instrument

		rP172[a] ($N = 2$)				rM179[a] ($N = 2$)			
pH[b]	T (°C)	$R_1 = R_2$ (nm)	R_3 (nm)	R_3/R_1	n	$R_1 = R_2$ (nm)	R_3 (nm)	R_3/R_1	n
8.1	4	12.2	5.5	0.45	57	12.3	5.7	0.46	55
7.9	4	12.0	5.3	0.44	48	12.2	5.5	0.45	52
7.8	25	12.6	6.4	0.51	70				
7.5	25	13.1	6.3	0.48	80	12.5	6.5	0.52	70
	mean	12.5	5.9	0.47	64	12.3	5.9	0.48	59
	max − min	1.1	1.1	0.07	32	0.3	1.0	0.07	18

[a] rP172 and rM179 in 2 mg/mL suspensions of 80 mM Tris-HCl buffer. [b] The pH values given in the table were measured at the given temperatures.

were found to be very well described by monodisperse (0%PD) oblate ellipsoids with a ratio of the shorter (= rotational) axis to the larger axis of about 0.45−0.5. Table 1 summarizes the SAXS results obtained using the ellipsoid model. Note that the mean values, which are averages of results for different pH and temperature conditions, are just listed to facilitate the comparison. The differences between the maximum and the minimum values for the size dimensions are relatively small as compared to these mean values. Hence, no major changes in size or shape were observed at pH values between 7.5 and 8.1 and temperatures of 4 and 25 °C. For both proteins, the smaller half axis lies in the range of 5−6 nm, whereas the larger half axis corresponds to 12−13 nm. We calculated that about 50−60 monomers assembled to build up one oblate at 4 °C. At 25 °C (and somewhat lower pH values) the evaluated number of monomers is in the range of 70−80. A typical volumetric thermal expansion of proteins in the range of 1×10^{-3}/K (see, e.g., ref 33), which was not taken into account for the evaluation at the two different temperatures, cannot explain the large difference of about 25%. Nevertheless, because the number of monomers was derived from extrapolating the SAXS curves to $Q \rightarrow 0$ and under the assumption that all the protein molecules build nanoparticles, these values should be interpreted with caution. It is possible that the large increase in the evaluated number of monomers between the two temperatures partially arises from structural rearrangements which are not visible in the accessible range of scattering angles.

Alternatively, a size distribution of spherical particles could as well be responsible for the fact that predicted oscillations, which are characteristic for monodisperse spheres, were not observed. Indeed, the experimental data seen in Figure 1 are also consistent with a size distribution of spherical particles. However, a very large polydispersity of 33% would be required for the predicted scattering curve to properly fit the experimental data (mean radius $R = 6.0$ nm, $\chi^2_{red} = 0.69$). As already mentioned in the Introduction, this high polydispersity would contradict previous DLS observations on the self-assembly of recombinant amelogenins at comparable pH values. Nevertheless, we performed additional DLS studies on samples that were prepared in exactly the same way as the ones used for the SAXS measurements to obtain supporting information on the polydispersity of the protein suspensions. The results are summarized in Table 2. Please note that the mean values, obtained by averaging over different conditions, cannot be assigned to any physical meaning and are just given for comparison. The polydispersity values for rP172 and rM179 obtained from DLS measurements are in the range of 10−17% for pH > 7.4, reflecting the experimental conditions used for the SAXS measurements reported in Table 1. This is just at the limit (15%) of what would still be considered monodisperse in DLS measurements and is much smaller than the 33% polydispersity required to support a SAXS model of polydisperse spheres. For comparison, we also tested a size distribution of spheres with a fixed polydispersity of 15% (fitted mean radius $R = 8.2$ nm). However, such a model did not give any satisfying solution ($\chi^2_{red} = 7.5$). Hence, the SAXS results together with the DLS findings clearly provide evidence for a deviation from a spherical shape.

Table 2. Polydispersity (PD) and Hydrodynamic Radii R_H of the Recombinant Amelogenins rP172 and rM179 Measured by Means of DLS

		rP172[a] ($N = 3$)		rM179[a] ($N = 2$)	
pH[b]	T (°C)	PD (%)	R_H (nm)	PD (%)	RH (nm)
8.03	7	17.0	14.7	16.2	14.9
7.95	10	15.4	13.8	10.1	14.2
7.87	13	17.0	13.3	13.5	14.0
7.78	16	14.7	13.3	15.7	13.7
7.70	19	16.0	13.2	15.2	13.7
7.61	22	15.5	13.8	12.8	13.8
7.53	25	17.1	14.7	14.1	13.6
7.45	28	16.8	17.2	14.3	15.1
7.36	31	18.3	22.6	17.9	17.3
7.28	34			20.7	26.3
	mean	16.4	15.2	15.0	15.7
	max − min	3.6	9.4	10.6	12.7

[a] rP172 and rM179 in 2 mg/mL suspensions of 80 mM Tris-HCl buffer adjusted to a pH of 7.2 at 37 °C. [b] pH values shown are calculated on the basis of the known temperature coefficient for Tris-HCl.

In addition to the polydispersity values, the DLS measurements also yielded information on the size of the protein agglomerates. The hydrodynamic radii of about 15 nm (see Table 2) are somewhat larger than the largest radius (longer half axis) of the ellipsoidal model based on the SAXS results (12−13 nm, Table 1). This difference will be discussed later on.

Being aware that the size and shape information obtained from the fit with a monodisperse (0%PD) oblate model (SAXS results in Table 1) might be affected by additional, superimposed effects of a size distribution with a moderate polydispersity, as obtained by means of DLS, we also tested a combination of the two approaches: oblate ellipsoids with $R_1 = R_2 = R$ and $R_3 = R\varepsilon$, as before, but now R has a size distribution with a fixed polydispersity of 15%. The experimental data shown in Figure 1 can be very well described by such a model ($\chi^2_{red} = 0.71$). The obtained aspect ratios differ by less than 10% ($\varepsilon = 0.49$ for 15%PD, $\varepsilon = 0.45$ for 0%PD). These results strongly confirm the finding on the oblate shape. The model that has just been described assumes that both size dimensions visible in SAXS (R, εR) have the same polydispersity as measured for the hydrodynamic radii using DLS. Because this assumption is not necessarily true, the alternative model should just be seen as a test allowing for taking into account the effect of a possible,

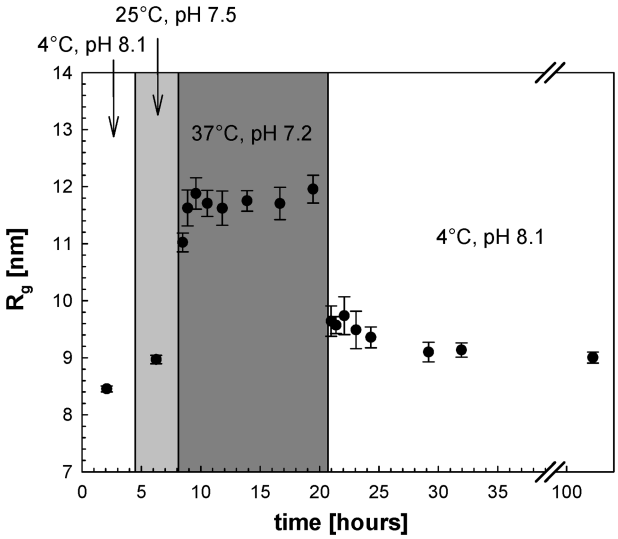

Figure 2. Radius of gyration R_g vs time determined from SAXS measurements (Nanostar laboratory instrument) of a 2 mg/mL suspension of rP172 prepared in 80 mM Tris-HCl buffer adjusted to pH 7.2 at 37 °C. The temperature dependence of the buffer was used to change the pH value by means of heating and cooling the sample. The boxes with different gray scales correspond to different temperatures and measured pH values. At pH 7.2, R_g shows a remarkable increase. Larger error bars indicate deviations from the Guinier approximation, which is only valid for well-separated particles.

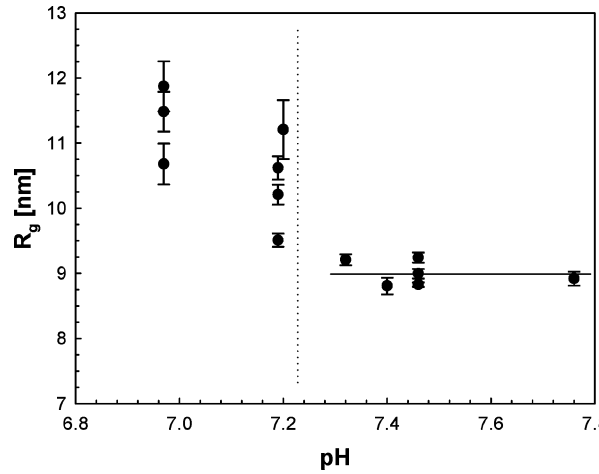

Figure 3. Radius of gyration R_g determined from SAXS measurements (Nanostar laboratory instrument) of rP172 (2 mg/mL) in 80 mM Tris-HCl buffers that were adjusted to different pH values. The temperature during all the measurements was 25 °C. The increase in R_g at pH values lower than pH 7.2 together with the increase in the size of the error bars results from a pH-induced aggregation of protein nanoparticles.

moderate polydispersity. A comparison between the two models supports the results obtained with the monodisperse (0%PD) oblate model.

Besides the shape of individual rP172 and rM179 nanoparticles, their aggregation at pH values close to physiological conditions, as described in the Introduction, is of major importance for directing the growth of hydroxyapatite crystals. Hence, we also studied pH-induced changes of amelogenin self-assembly in suspension. The radius of gyration R_g was chosen as a size parameter for the comparison of the SAXS profiles at varying pH and temperature combinations. R_g averages all the dimensions of the particle and is given by $R_g = R\sqrt{2+\varepsilon^2/5}$ for ellipsoids of revolution with the aspect ratio ε.[27] Figure 2 shows the changes in R_g versus time during a series of measurements taken while a change in pH was induced (see Materials and Methods) through the heating and cooling of a 2 mg/mL suspension of rP172 prepared in Tris-HCl buffer.

Due to the large temperature dependence of the Tris-HCl buffer, the different temperatures correspond to different pH values. At 4 °C and pH 8.1, the rP172 agglomerates had a radius of gyration of 8.5 nm. During heating of the suspension and, therefore, decreasing pH values, R_g increased. First, R_g rose a moderate 6%, as the pH decreased from pH 8.1 to pH 7.5. However, R_g then rose by the considerable amount of 23%, as the pH was further decreased from pH 7.5 at 25 °C to pH 7.2 at 37 °C. After this abrupt change at 37 °C and pH 7.2, R_g remained constant. The relatively large error bars for the radii at pH 7.2 are due to deviations from the Guinier approximation which is only valid for diluted systems, where the particles are well separated from each other. This behavior indicates an aggregation of the amelogenin nanoparticles at pH 7.2. The data measured for pH 7.2 could also not be fitted with the model of isolated oblate ellipsoids. After cooling down to 4 °C (pH 8.1) we observed a sudden decrease of R_g toward its original lower level.

To distinguish pH-induced changes from temperature effects, we tested protein suspensions in different buffer solutions. Figure 3 shows the effect of changes in pH on the R_g of rP172 at a constant temperature of 25 °C. At pH values higher than pH 7.2, the evaluated R_g of rP172 remained at a constant level of about 9 nm. In contrast, at lower pH values, the radii increased markedly on average (between pH 7.2 and pH 6.9), although showing rather large differences between separate measurements and larger error bars than those found at pH > 7.2. These variations indicate the beginning of an aggregation of the nano-oblates, with decreasing pH. Of note, the data shown in Figure 3 that were obtained at 25 °C reveal that this transition takes place at the same pH value (i.e., pH 7.2) that was observed for experiments carried out at 37 °C (as shown in Figure 2) despite the difference in temperature. For rM179 we observed the same behavior as for rP172, with an onset of aggregation close to pH 7.2.

All of the results shown above were measured for suspensions with a constant concentration of 2 mg/mL. Using an ultrasound trap to levitate a droplet of an amelogenin suspension enabled us to perform in situ synchrotron SAXS experiments while increasing the protein concentration by means of solvent evaporation. Figure 4 shows the time dependence of the R_g and the protein concentration during a measurement of rP172 at 20 °C in a suspension with an initial concentration of 2 mg/mL and an initial pH value of 7.9. Because the Tris-HCl buffer concentration also increased during the evaporation, the pH of the sample presumably changed toward elevated pH values during the experiment. The radii were evaluated from the SAXS data, whereas the concentrations were calculated assuming a linear decrease of the droplet radius with time. Interestingly, even though the concentration increased quite considerably, R_g remained constant. Only shortly before drying completely, the evaluated radii showed a sudden change (Figure 4). Furthermore, the shape of the scattering curves (not shown) and, hence, the shape of the nano-oblates did not change until shortly before drying. It is possible that the individual oblates aggregated into higher order structures (e.g., chains) when the concentration was increased. However, the resolution of the used setup did not allow for studying the aggregation behavior.

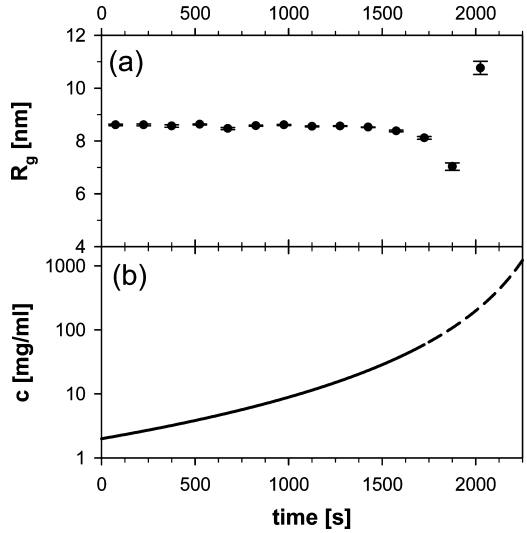

Figure 4. (a) Radius of gyration R_g determined from in situ synchrotron SAXS measurements (μ-Spot beamline, BESSY II, HZB) of rP172 at 20 °C and a measured pH value of 7.9 and (b) calculated concentration c of the protein suspension vs time. A 5 μL droplet without any sample container was levitated by using an ultrasound trap. Solvent evaporation led to an increase in the concentration, but R_g was not affected over a wide range of concentrations. At very high protein concentrations, shortly before drying, the evaporation rate presumably differs from the function used to calculate the concentration (see also Materials and Methods). Hence, these values (dashed part of the curve) should only be seen as rough estimates.

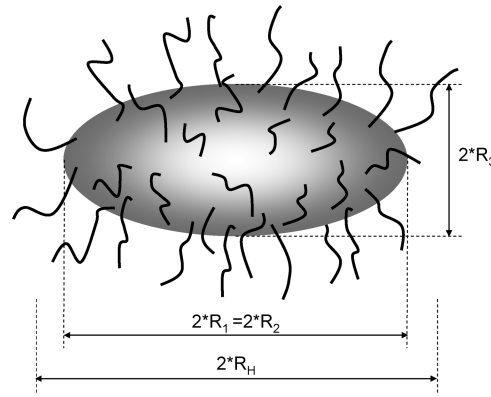

Figure 5. Revised core−shell model for the structure of amelogenin nanoparticles based on SAXS and DLS measurements of rP172 and rM179 at pH > 7.2. The SAXS measurements reflect the dimensions of the more electron-dense oblate core ($R_1 = R_2$, R_3), whereas the hydrodynamic radius R_H describes the overall size, including the loose shell, which affects the mobility of the particle as measured by means of DLS. The scheme is consistent with the radii given in Tables 1 and 2.

Discussion

Although amelogenin agglomerates in suspension have usually been referred to as nanospheres,[34] our combined SAXS and DLS findings on rP172 and rM179 in aqueous solutions at pH values higher than pH 7.2 suggest a nonspherical, oblate shape with an aspect ratio of 0.45−0.5. SAXS is not a dynamic measurement and averages over long acquisition times (hours for the laboratory measurements). Therefore, the oblate shape represents the average structure of the amelogenin agglomerates which may well be flexible in nature. To the best of our knowledge, the current study provides for the first time quantitative results showing that recombinant amelogenins form oblate rather than spherical particles in suspension, using an approach that avoids potential artifacts that may result when such particles are in contact with support materials (e.g., mica, TEM grid or similar) typically used for AFM and TEM analyses.

The difference in the hydrodynamic radii as measured by DLS and the largest dimension of the particles as measured by means of SAXS, can be explained by a dense core and a loose shell model of the monodisperse nano-oblates (see Figure 5). The hydrophilic loose shell affects the mobility that is measured by means of DLS but is not visible by SAXS, where the signal is dominated by the hydrophobic core with much higher electron density. This finding is in agreement with our previous DLS and SAXS studies on rM179.[18] Additionally, the results of our current study strongly support a model of monodisperse amelogenin nanoparticles with an oblate core. The amphiphilic nature of the investigated full-length recombinant amelogenins and the folding of the proteins apparently favor the formation of oblate nanoparticles. The similarity in shape and behavior observed between rP172 and rM179 is consistent with the fact that their primary structures are highly homologous, with nearly identical N- and C-terminal domains.[1,3]

Deviations from a spherical shape have previously also been reported for amphiphilic copolymers, which assemble into micellar structures with a dense core and a less dense corona, similar to the structure of the amelogenin nanoparticles. Depending on the chemical composition of the polymers not only spherical cores but also oblate[35] or prolate[36] ellipsoidal core structures were observed by means of SAXS.

Importantly, the oblate shape of amelogenin nanoparticles may be of critical importance as it contributes to the explanation for their assembly into anisotropic higher-order elongated (i.e., chain-like and fiber-like) structures, observed in vitro,[17,19–21] and predicted from SAXS/DLS data.[18] For high volume fractions of amelogenin nanoparticles, as present in the forming enamel, the oblate shape presumably induces an arrangement with a preferred orientation. This would favor an aggregation in preferred directions as compared to the formation of a randomly connected network. Furthermore, the anisometric dimensions suggest asymmetries in the surface properties of the particles such as local variations in the surface charge. If special parts of the surface of the oblate particles showed different electrostatic interactions, this would also induce a directionality of the aggregation. For instance, repulsive forces between equally charged surfaces on the flat part of the oblates or pronounced attractive interactions between their more curved sides would lead to a side by side assembly of the amelogenin oblates. This could be an explanation for the above-mentioned TEM and AFM observations of chain-like structures. Consistent with the need for charge heterogeneity, the formation of such elongated assemblies was shown for the full-length amelogenin and not for cleaved amelogenins that lack the hydrophilic C-terminus in several studies.[18–21] The full-length molecule contains the charged hydrophilic C-terminal domain that differs markedly from the remainder of the molecule that is primarily hydrophobic. In a recent study, however, elongated assemblies were observed by AFM to form over several days from dilute suspensions (0.1 mg/mL total protein) of both recombinant full-length (rH174) and truncated (rH163: that lacks 11 C-terminal amino acids) human amelogenin, and their mixtures, at specified pH values.[37] The authors of the latter study concluded that assembly was primarily driven by the distribution of charge on the surfaces of amelogenin nanoparticles, as we suggest based on our present findings on the self-assembly of full-length amelogenin in solution. Further investigations will be necessary to find out if and how the oblate shape and possible variations in the surface charge affect the aggregation of amelogenin

nanoparticles. Hence, additional imaging and scattering studies are underway to address the hypothesis that the oblate structure plays an important role in the formation of linear chain-like amelogenin aggregates.

Besides providing information on the shape of individual, isolated amelogenin nanoparticles, SAXS results have also allowed us to identify the conditions for the further assembly of the nano-oblates into high-order elongated structures. We would like to point out that the temperature and pH changes that we used to perturb our in vitro system in a controlled way are not intended to mimic similar changes in the biological process. Instead, this approach was only applied to determine the final pH values and temperatures for which an aggregation of the nano-oblates can be found. Previously, we reported on a temperature-induced aggregation process for the recombinant amelogenin rM179 and showed differences in the aggregation of the full-length protein rM179 and the truncated protein rM166. However, the Tris-HCl buffer used in that study[18] had a strong temperature dependence and the effect of pH was not systematically investigated. More recently, published DLS and TEM studies which took into account the temperature dependence of the buffers used indicated that the in vitro assembly of recombinant amelogenins is pH-triggered rather than temperature-dependent.[19] In very good agreement with these findings, our current SAXS study again shows a sharp transition point at a well-defined pH value of pH 7.2 (Figures 2 and 3) for full-length recombinant amelogenins, despite differences in temperature. At higher pH values, the investigated amelogenins build isolated nano-oblates, as supported by the fitting of appropriate shape models to the SAXS data (Figure 1) and the derived model parameters (Table 1). At pH values lower or equal to this limit the nano-oblates start to aggregate (see Figures 2 and 3). These results provide additional evidence that the assembly into higher-order structures is mainly controlled by the pH value. By raising the pH after keeping the protein suspensions at pH 7.2 for several hours, we also found that, to a large degree, the aggregation process is reversible. The scattering profiles obtained after raising the pH value were again in agreement with a model of isolated oblate particles. Moreover, a quantitative analysis shows that the initial dimensions before the aggregation were almost fully restored. Hence, the aggregation of the nano-oblates at pH values close to pH 7.2 and temperatures from 25 to 37 °C is at least partially reversible. This finding contradicts previous observations[18] where the aggregation of rM179 was found to be nonreversible, however, at the much higher temperature of 46 °C. The higher temperature presumably induced nonreversible structural rearrangements which were not observed for lower temperatures up to 37 °C.

Finally, the results obtained with the ultrasound trap (Figure 4) demonstrate that the amelogenin nano-oblates do not significantly change in size and shape, even if the concentration of the suspension is dramatically increased up to more than 60 mg/mL. This finding supports the hypothesis that the results discussed above, which were obtained using relatively low amelogenin concentrations of 2 mg/mL, are not only relevant for diluted in vitro systems but also for the early (secretory) stages of enamel formation in vivo where concentrations of enamel matrix proteins (90% amelogenins) are considerably higher. The in vivo concentration of enamel matrix proteins has been reported to be 200−300 mg/mL.[38,39] Furthermore, in agreement with our new SAXS observations, previous AFM studies[22] revealed that even amelogenin gels consist of assembled amelogenin nanoparticles similar to the ones found in suspensions.

When comparing our in vitro studies with the in vivo situation, one should also keep in mind that the protein in vivo does not self-assemble independently, but is under the influence of initial mineralization events and growing mineral crystals. In vitro mineralization studies have confirmed the hypothesis that amelogenins are able to promote the formation of aligned, elongated hydroxyapatite crystals.[17,40,41] Importantly, however, it was found that growing mineral crystals are only aligned when the assembly of the protein and the growth of the crystals occur simultaneously.[3,17] NMR studies on a truncated amelogenin (LRAP) and its structure in the presence of hydroxyapatite (HA) crystals have shown that its entire C-terminal domain is involved in binding amelogenins to HA surfaces.[42,43] However, amelogenins lacking the hydrophilic C-terminus have also been shown to interact with growing calcium phosphate crystals, affecting their shape and size.[3,17,44,45] Nevertheless, considering that the charged C-terminal is of high relevance for both protein−mineral and the protein−protein interactions between the nano-oblates, the growth of the mineral crystals during the early stages of enamel formation will most likely affect the self-assembly behavior of the full-length amelogenin in vivo. The current in vitro study does not take into account the influence of mineral crystals and cells, as present in the developing enamel. Elongated HA crystals, interacting with amelogenins during the formation of enamel, presumably even enhance the tendency of the protein to assemble into elongated, chain-like structures. Moreover, in the in vivo situation, a phosphate group at serine residue 16, which is lacking in the investigated recombinant proteins rP172 and rM179, might also play an important role for the interaction of amelogenins with HA mineral and their self-assembly. In spite of these differences, the finding that recombinant full-length amelogenins intrinsically form anisometric nanoparticles which can assemble into anisotropic higher-order structures highlights amelogenins as especially well-suited for guiding the mineralization of enamel.

Conclusion

This study on the self-assembly of full-length recombinant amelogenins rP172 and rM179 in suspensions provides new evidence for an oblate shape for amelogenin nanoparticles, that have been previously described as nanospheres, and their further aggregation at pH values close to those found under physiological conditions.[5,6] We propose that the observed anisometric shape of full-length amelogenin nanoparticles in suspension is a key factor associated with the formation of higher-order anisotropic chain-like structures. These structures are believed to play a critical role in regulating the organization of enamel crystals on the nanoscale, resulting in the parallel arrangement of elongated hydroxyapatite crystals. In addition to providing new insights into the mechanisms behind the biomineralization of dental enamel, our results should aid in the development of bioinspired materials and approaches for enamel repair and regeneration.

Acknowledgment. We are grateful to Ingrid Zenke, Stefan Siegel, and Chenghao Li for the support during the lab SAXS experiments and the synchrotron SAXS experiments that were performed at the μ-spot beamline at BESSY II (Berlin, Germany). This work was supported by Grant DE-016376 (HCM) from the National Institute of Dental and Craniofacial Research (NIDCR). F.B.W.-B. was also partially supported by Grant T32 DE-007327 from the NIDCR.

References and Notes

(1) Fincham, A. G.; Moradian-Oldak, J.; Simmer, J. P. *J. Struct. Biol.* **1999**, *126* (3), 270–299.

(2) Paine, M. L.; White, S. N.; Luo, W.; Fong, H.; Sarikaya, M.; Snead, M. L. *Matrix Biol.* **2001**, *20* (5−6), 273–292.
(3) Margolis, H. C.; Beniash, E.; Fowler, C. E. *J. Dent. Res.* **2006**, *85* (9), 775–793.
(4) Zeichner-David, M. *Matrix Biol.* **2001**, *20* (5−6), 307–316.
(5) Aoba, T.; Moreno, E. C. *Calcif. Tissue Int.* **1987**, *41* (2), 86–94.
(6) Smith, C. E.; Issid, M.; Margolis, H. C.; Moreno, E. C. *Adv. Dent. Res.* **1996**, *10*, 159–169.
(7) Bartlett, J. D.; Ryu, O. H.; Xue, J.; Simmer, J. P.; Margolis, H. C. *Connect. Tissue Res.* **1998**, *39* (1−3), 405–413.
(8) Smith, C. E.; Nanci, A. *Anat. Rec.* **1996**, *245* (2), 186–207.
(9) Uchida, T.; Tanabe, T.; Fukae, M.; Shimizu, M.; Yamada, M.; Miake, K.; Kobayashi, S. *Histochemistry* **1991**, *96* (2), 129–138.
(10) Robinson, C.; Fuchs, P.; Weatherell, J. A. *J. Cryst. Growth* **1981**, *53* (1), 160–165.
(11) Fincham, A. G.; Moradian-Oldak, J.; Simmer, J. P.; Sarte, P.; Lau, E. C.; Diekwisch, T.; Slavkin, H. C. *J. Struct. Biol.* **1994**, *112* (2), 103–109.
(12) Moradian-Oldak, J.; Simmer, J. P.; Lau, E. C.; Sarte, P. E.; Slavkin, H. C.; Fincham, A. G. *Biopolymers* **1994**, *34* (10), 1339–1347.
(13) Fincham, A. G.; J.; Moradian, O.; Diekwisch, T. G. H.; Lyaruu, D. M.; Wright, J. T.; Bringas, P., Jr.; Slavkin, H. C. *J. Struct. Biol.* **1995**, *115* (1), 50–59.
(14) Moradian-Oldak, J.; Leung, W.; Fincham, A. G. *J. Struct. Biol.* **1998**, *122* (3), 320–327.
(15) Moradian-Oldak, J.; Paine, M. L.; Lei, Y. P.; Fincham, A. G.; Snead, M. L. *J. Struct. Biol.* **2000**, *131* (1), 27–37.
(16) Wen, H. B.; Fincham, A. G.; Moradian-Oldak, J. *Matrix Biol.* **2001**, *20* (5−6), 387–395.
(17) Beniash, E.; Simmer, J. P.; Margolis, H. C. *J. Struct. Biol.* **2005**, *149* (2), 182–190.
(18) Aichmayer, B.; Margolis, H. C.; Sigel, R.; Yamakoshi, Y.; Simmer, J. P.; Fratzl, P. *J. Struct. Biol.* **2005**, *151* (3), 239–249.
(19) Wiedemann-Bidlack, F. B.; Beniash, E.; Yamakoshi, Y.; Simmer, J. P.; Margolis, H. C. *J. Struct. Biol.* **2007**, *160* (1), 57–69.
(20) Du, C.; Falini, G.; Fermani, S.; Abbott, C.; Moradian-Oldak, J. *Science* **2005**, *307* (5714), 1450–1454.
(21) Moradian-Oldak, J.; Du, C.; Falini, G. *Eur. J. Oral Sci.* **2006**, *114*, 289–296.
(22) Wen, H. B.; Moradian-Oldak, J.; Leung, W.; Bringas, P.; Fincham, A. G. *J. Struct. Biol.* **1999**, *126* (1), 42–51.
(23) Simmer, J. P.; Lau, E. C.; Hu, C. C.; Aoba, T.; Lacey, M.; Nelson, D.; Zeichner-David, M.; Snead, M. L.; Slavkin, H. C.; Fincham, A. G. *Calcif. Tissue Int.* **1994**, *54* (4), 312–319.
(24) Paris, O.; Li, C. H.; Siegel, S.; Weseloh, G.; Emmerling, F.; Riesemeier, H.; Erko, A.; Fratzl, P. *J. Appl. Crystallogr.* **2007**, *40*, S466–S470.
(25) Leiterer, J.; Emmerling, F.; Panne, U.; Christen, W.; Rademann, K. *Langmuir* **2008**, *24* (15), 7970–7978.
(26) Orthaber, D.; Bergmann, A.; Glatter, O. *J. Appl. Crystallogr.* **2000**, *33*, 218–225.
(27) Guinier, A.; Fournet, G. *Small-Angle Scattering of X-Rays*; John Wiley and Sons: New York, 1955.
(28) Pedersen, J. S. *Adv. Colloid Interface Sci.* **1997**, *70*, 171–210.
(29) Fischer, H.; Polikarpov, I.; Craievich, A. F. *Protein Sci.* **2004**, *13* (10), 2825–2828.
(30) Ryu, O. H.; Fincham, A. G.; Hu, C. C.; Zhang, C.; Qian, Q.; Bartlett, J. D.; Simmer, J. P. *J. Dent. Res.* **1999**, *78* (3), 743–750.
(31) Habel, J. E.; Ohren, J. F.; Borgstahl, G. E. O. *Acta Crystallogr., Sect. D: Biol. Crystallogr.* **2001**, *57*, 254–259.
(32) Bergfors, T. *Protein Crystallization: Techniques, Strategies, and Tips*; International University Line: La Jolla, CA, 1999; p 300.
(33) Mitra, L.; Oleinikova, A.; Winter, R. *ChemPhysChem* **2008**, *9* (18), 2779–2784.
(34) Moradian-Oldak, J. *J. Dent. Res.* **2007**, *86* (6), 487–490.
(35) Zhou, Z. L.; Li, Z. B.; Ren, Y.; Hillmyer, M. A.; Lodge, T. P. *J. Am. Chem. Soc.* **2003**, *125* (34), 10182–10183.
(36) Pedersen, J. S.; Hamley, I. W.; Ryu, C. Y.; Lodge, T. P. *Macromolecules* **2000**, *33* (2), 542–550.
(37) He, X. D.; Li, W.; Habelitz, S. *J. Struct. Biol.* **2008**, *164* (3), 314–321.
(38) Fukae, M. *Symposium of Oral Science*; Tsurumi University School of Dental Medicine: Yokohama, Japan, 2002; pp 73−78.
(39) Robinson, C.; Kirkham, J.; Hallsworth, A. S. *Arch. Oral Biol.* **1988**, *33* (3), 159–162.
(40) Iijima, M.; Moradian-Oldak, J. *Biomaterials* **2005**, *26* (13), 1595–1603.
(41) Habelitz, S.; Kullar, A.; Marshall, S. J.; DenBesten, P. K.; Balooch, M.; Marshall, G. W.; Li, W. *J. Dent. Res.* **2004**, *83* (9), 698–702.
(42) Shaw, W. J.; Ferris, K. *J. Phys. Chem. B* **2008**, *112* (51), 16975–16981.
(43) Shaw, W. J.; Ferris, K.; Tarasevich, B.; Larson, J. L. *Biophys. J.* **2008**, *94* (8), 3247–3257.
(44) Iijima, M.; Moriwaki, Y.; Takagi, T.; Moradian-Oldak, J. *J. Cryst. Growth* **2001**, *222* (3), 615–626.
(45) Iijima, M.; Moriwaki, Y.; Wen, H. B.; Fincham, A. G.; Moradian-Oldak, J. *J. Dent. Res.* **2002**, *81* (1), 69–73.

BM900983B